J Therm Spray Tech (2021) 30:1093–1106
https://doi.org/10.1007/s11666-021-01188-w

PEER REVIEWED

Numerical Analysis of Deformation Behavior and Interface Bonding of Ti6Al4V Particle After Subsequent Impact During Cold Spraying

Hongxia Zhou[1] · Chengxin Li[2] · Chris Bennett[3] · Hussain Tanvir[4] · Changjiu Li[2]

Submitted: 15 August 2020 / in revised form: 8 January 2021 / Accepted: 14 February 2021 / Published online: 25 March 2021

Abstract During cold-spraying processes, the deposited particles play a crucial role owing to the subsequent particle collisions with surface. Herein, using finite-element modeling, we numerically analyze the particle behavior under three models: impact of a single Ti6Al4V (TC4) particle, deposited particle hammered by a subsequent TC4 particle, and deposited particle impacted by a large shot peening particle (SP). For the single TC4 particle case, the particle deformation was limited and maximum interface temperature of the particle was lower than its melting point. The high-temperature region was mainly distributed in a limited area near the particle edge. Meanwhile, for subsequent impact in the second TC4 particle case, the upper half of previously deposited particle was deformed, although the change in maximum interface temperature was minimal. However, for particles subsequently impacted by large peening particle, the deformation of previously deposited TC4 particles increased significantly, and the temperature, both adjacent to and opposite the interface, exceeded the melting point of the titanium alloy in a large surface area, indicating that localized interfacial melting has occurred. In the third case, the change in interface temperature, stress, and energy with time, along with the experimental results, suggests that the bond between the particle and substrate enhanced.

Keywords cold spraying · local melting · shot peening · simulation · Ti6Al4V

Introduction

Cold gas dynamic spray is a rapid fabrication process where micron-sized solid powders are accelerated by an expanding gas stream to impact and then adhere to a substrate (Ref 1, 2). During cold spraying, substantial plastic deformation occurs in the particle and substrate, causing the thin oxide film on the surface of the particles and substrate to break. Then, fresh metal is splattered in a jet shape, which subsequently bonds with each other. At present, there are a number of studies that have been carried out to understand the bonding mechanism in cold spraying (Ref 3-7). Although the adiabatic shear instability theory can reasonably explain some phenomena observed during particle collisions when cold spraying, the bonding mechanism of cold-sprayed coatings remains poorly understood.

Some scholars believe that the impact of subsequent particles plays an important role in the deformation and bonding state of deposited particles (Ref 8, 9). In cold spraying, bonds will successfully form only if the particle velocity exceeds a critical value (Ref 10-12). Below this velocity, impacting particles will only cause densification and abrasion of the substrate or deposited coating, similar to shot peening (Ref 12). Because of this phenomenon, it is

✉ Chengxin Li
licx@mail.xjtu.edu.cn

[1] Qinghai Provincial Key Laboratory of New Light Alloys, Qinghai Provincial Engineering Research Center of High Performance Light Metal Alloys and Forming, Qinghai University, Xining 810016, People's Republic of China

[2] State Key Laboratory for Mechanical Behavior of Materials, School of Materials Science and Engineering, Xi'an Jiaotong University, Xi'an, Shanxi 710049, People's Republic of China

[3] Gas Turbine and Transmissions Research Group, Faculty of Engineering, University of Nottingham, Nottingham NG7 2RD, UK

[4] Advanced Materials Research Group, Faculty of Engineering, University of Nottingham, Nottingham NG7 2RD, UK

reasonable to use the external force of the following particles to further deform the lightly deformed particles. Since the critical velocity of particles increases with particle size, the in situ peening effect of large particles can be used to assist in the deformation of difficult-to-deform metals, e.g., Ti and Ti alloys. Some studies have reported that dense Ti and TC4 coatings can be obtained in situ through shot peening-assisted cold spraying (Ref 13), in which large stainless steel particles were mixed into spraying powders. The Ti and TC4 particles bond with the substrate or already deposited particles while the impulse delivered by large stainless steel particles tamp them further. The steel particles rebound because they are beneath their critical velocity. Figure 1 presents the schematic diagram for the in situ shot peening-assisted cold spraying. The adhesion strength under in situ shot peening was similarly enhanced compared with traditional spraying (Ref 14).

In cold spraying, the impact-driven deformation of particles is completed within tens of nanoseconds and the high-speed collision process transient with a strain rate is as high as 10^{10} s^{-1} (Ref 1, 9, 11); therefore, it is difficult to directly observe the deformation process (Ref 7, 15). As a more achievable means of investigation, numerous finite-element analysis (FEA) studies have been performed to examine the impact-deformation process during cold spraying (Ref 16). ABAQUS/explicit is a commonly used finite-element software for simulating the impact process when cold spraying. The Lagrangian method is often used to simulate the deformation behavior of the particle and the substrate (Ref 6, 7, 12, 17-22). At present, there are many studies that have studied the deformation of a single particle after impact using this method (Ref 6, 7, 12, 20-22). In a work by Assadi et al. (Ref 12) on copper cold-spraying processes, the concept of adiabatic shear instability was first proposed to explain the result in which an abrupt increase in local temperature or equivalent plastic strain (PEEQ) occurred. This theory is widely accepted because it can explain the edge jetting of impacting particles and their bonding behavior during cold spraying. However, due to the high strength of Ti and Ti alloys, it is very hard for them to deform during the cold spraying, and the porous microstructure and weak bonding between particles result in low strength and durability when used for cold-spray alloys coatings. Likewise, traditional adiabatic shear instability theory does not fit Ti and Ti alloy coatings well since there is no severe deformation and rim jetting. Bae et al. (Ref 7) proposed the interfacial melting theory to explain the bonding features observed between Ti particles and demonstrated that the impact temperature in the substrate–particle interface exceeded the melting point of Ti through numerical simulation. They believed that it resulted from the relatively higher adiabaticity of Ti when compared with other materials. However, their work only focused on particle deformation and interface temperature when the particle deposits on the substrate and did not consider the role of subsequent particle impacts. To date, no relevant numerical simulation work has been carried out on the cold spray impact behavior of in situ shot peening-assisted cold spraying. To thoroughly comprehend the deformation behavior of particles under microscopic external force, we constructed three models and numerically analyzed the deformation behavior of the target TC4 particle in each case: impact of a single Ti6Al4V (TC4) particle, a deposited particle hammered by a subsequent TC4 particle, and a deposited particle impacted by a large shot peening particle. Finally, we compared the results with those of single TC4 particle deposition studies and summarized the deformation characteristics of previously deposited TC4 particles.

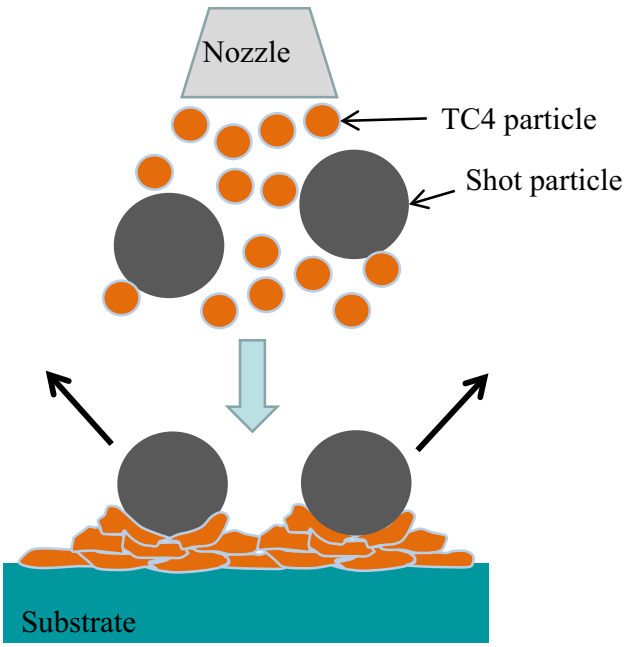

Fig. 1 Schematic diagram of in situ shot peening-assisted cold spraying

Computational Descriptions

Numerical Model

Nonlinear FEA simulations were performed using ABAQUS/explicit and a Lagrangian algorithm to simulate the deformation processes that would occur during cold spraying. All the three considered models were assumed to be an adiabatic process, and a dynamic explicit procedure was performed to conduct an adiabatic stress analysis. Due to the axisymmetric character of a single particle impact,

the three models were simplified as 2D axisymmetric models, which are computationally more efficient and involved fewer artificial controls compared with 3D models (Ref 12, 23). The TC4 particle and shot peening particle had diameters (D_p) of 22 and 180 μm, respectively. This size was consistent with the average powder size used in our previous experiment (Ref 14), so that the present simulation results could be compared with the past experimental results. The radius and height of the substrate were defined as three and four times larger than the particle diameter, and the contact type between particle and the substrate was all treated as the "surface-to-surface contact" type; the friction coefficient of the contact surface was set to 0.3. The geometries were partitioned by four-node bilinear axisymmetric quadrilateral elements with reduced integration and hourglass control (CAX4RT). The size of the mesh in the TC4 particle and the center of the substrate was 1/50 D_p. As the deformation of the shot peening particle during the impact process is negligible, it does not require the same resolution and its mesh size was set to 1/10 D_p. The axisymmetric condition was applied and a fixed boundary condition was enforced to the bottom and sides. The initial temperature of TC4 and shot peening particles, as well as substrate, was set to 25 °C, and substrate heating by the process gas can be considered negligible (Ref 15, 24). Figure 2 shows a visualization of the mesh division in a two-dimensional computing model. The asterisk in Fig. 2(a) represents the node selected to study interface temperature and strain in the area of the particle periphery and occurs at an angle of 64.6° from the particle axis. The strain detection paths were performed in order from A to C. Corresponding experimental conditions for the simulation used N_2 as the process gas for spraying, and the gas temperature and pressure were 550 °C and 3 MPa, respectively. According to the results of previous research (Ref 13), under these experimental conditions, the velocities of the TC4 particle and shot particle were set to 700 and 300 m/s, respectively.

Material Model

The materials of the particle and substrate were described using a Johnson–Cook plasticity model which allows us to account for strain, strain rate hardening, and thermal softening (Ref 25). The stress is expressed according to the von Mises plasticity model, and the yield stress (σ_y) of the material is expressed as follows:

$$\sigma = \left[A + B\varepsilon_P^n\right]\left[1 + C\ln\dot{\varepsilon}^*\right]\left[1 - \left(\frac{T - T_{\text{ref}}}{T_{\text{melt}} - T_{\text{ref}}}\right)^m\right] \quad \text{(Eq 1)}$$

where A, B, N, C, and M are material-related constants, ε_p is the effective plastic strain, and ε^* is the effective plastic strain rate normalized with respect to a reference strain rate. T_{melt} is the melting temperature and T_{ref} is a reference temperature above which thermal softening can occur. A linear Mie-Grüneisen equation of state (EoS) was employed for studying elastic behavior (Ref 26). The properties of the TC4 material used in this study are listed in Table 1. These material parameters were derived from the literature (Ref 27-30).

In this study, isotropic TC4 was selected as the material of the particle and the substrate, and stainless steel was the shot material because in in situ shot peening-assisted cold spraying, the deformation of shot was very small and can be ignored. Therefore, conventional parameters, such as density (7.92 g/cm^3), elastic modulus (190 GPa), and Poisson's ratio (0.305) were set for the stainless steel particle. For the thermal conversion ratio, the default value

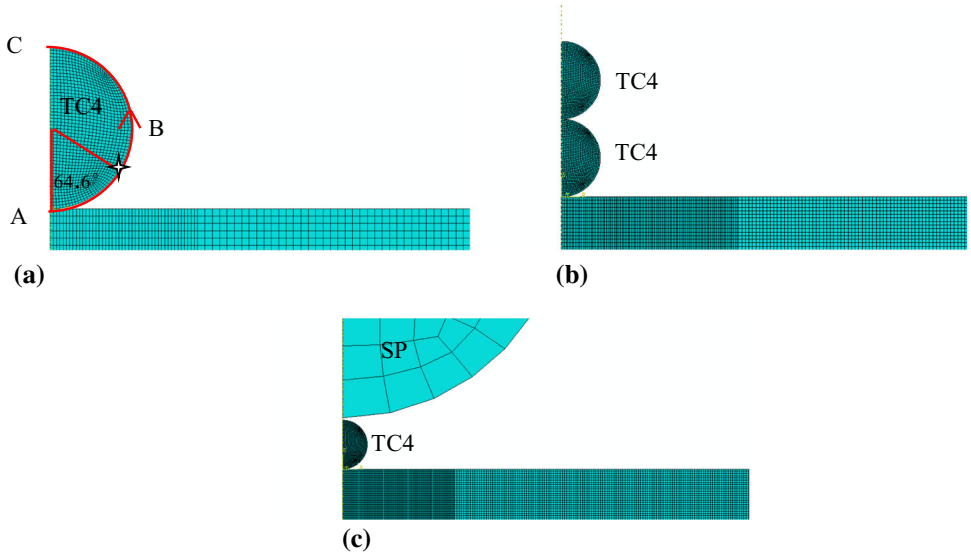

Fig. 2 2D axisymmetric models and mesh for particle/substrate impact simulation. (a) TC4 particle/TC4 substrate. (b) Two TC4 particles/TC4 substrate. (c) TC4 particle and shot particle/TC4 substrate

Table 1 Material properties used in FE models (Ref 27-30)

Parameter	Value
Density, kg/m^3	4428
Heat capacity, J/kg K	560
Shear modulus, GPa	41.9
Poison's ratio	0.31
A, MPa	1098
B, MPa	1092
N	0.93
C	0.014
M	1.1
Elastic bulk wave velocity, km/s	5.13
Slope in u_s, v_s, u_p diagram	1.028
Gür neisen coefficient	1.23
Melting temperature, K	1878
Reference temperature, K	298
Heat fraction	1

for general materials is 0.9, but due to the lower thermal conductivity of Ti and Ti alloys, it can be set to 1 (Ref 31).

Results

Deformation Behavior

Figure 3 shows the equivalent plastic strain of a single TC4 particle impacting the substrate and being subsequently impacted by either a TC4 particle or a shot particle. The impact times were 23, 48, and 77 ns, respectively. It can be seen that in the case of a single particle impact, the TC4 particle underwent limited deformation and the maximum equivalent plastic strain value was 2.05; moreover, there was no jetting phenomenon at the edge of the particle. This was mainly a result of the inflexibility of the Ti alloy. In reported experimental work on single TC4 particles (Ref 32), no distinct jet phenomenon was observed on the edge of the single deposited TC4 particles, but the morphology of the particle back surface showed that there was still metallurgical bonding between particle and substrate. Therefore, it can be concluded that there is no direct connection between rim sputtering and interface bonding for Ti and Ti alloy coatings. When a subsequent TC4 particle impacted on a deposited TC4 particle, the deposited particle was further tamped and deformed again (as shown in Fig. 3b, the subsequent TC4 particle is hidden). The highest equivalent plastic strain reached 3.34, which was slightly increased over the case of the single particle. When the large shot particle impacted the already deposited TC4 particle, it underwent secondary deformation and became completely flat (as shown in Fig. 3c, the shot particle is hidden). The equivalent plastic strain value of the particle rose rapidly, reaching maximum value of 39.14. Comparing the deformation characteristics of the deposited TC4 particle in the three cases, it can be clearly seen that the secondary hammering effect of the shot particle had significant influence on the particle deformation, and the deformation changed from the lower half of the particle to the whole. Compared with that tamped by an incident TC4 particle, in which the upper half of the particle was also deformed, the flattening degree of the deposited particle was not very high. Nevertheless, after the impact of the shot particle, the flattening degree was greatly improved, resulting in a rapid increase in the contact area between the deposited TC4 particle and the substrate, which will play a positive role in improving the adhesion.

Figure 4 shows the compression ratio and flattening ratio of previously deposited TC4 particle under the three conditions. The compression ratio is the ratio of the deformed

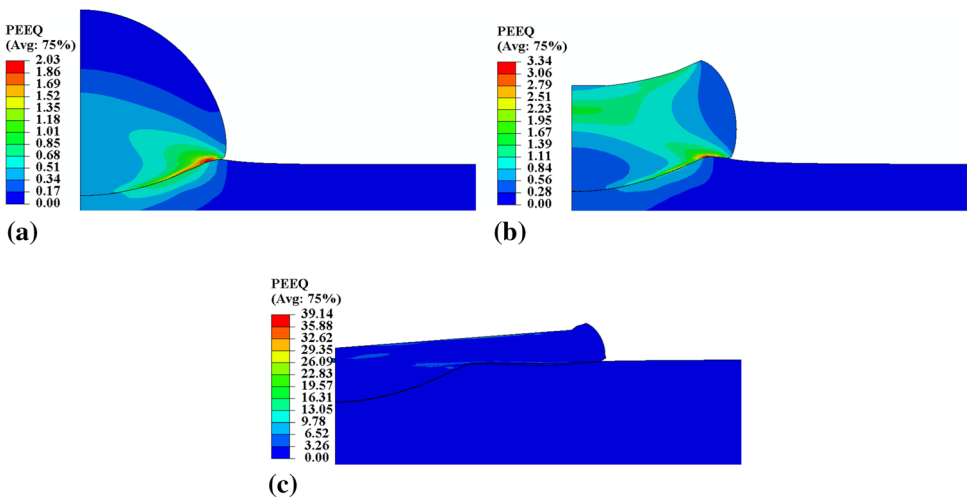

Fig. 3 PEEQ contour under three cases. (a) TC4 particle/TC4 substrate. (b) Impacted by subsequent TC4 particle. (c) Impacted by subsequent shot particle

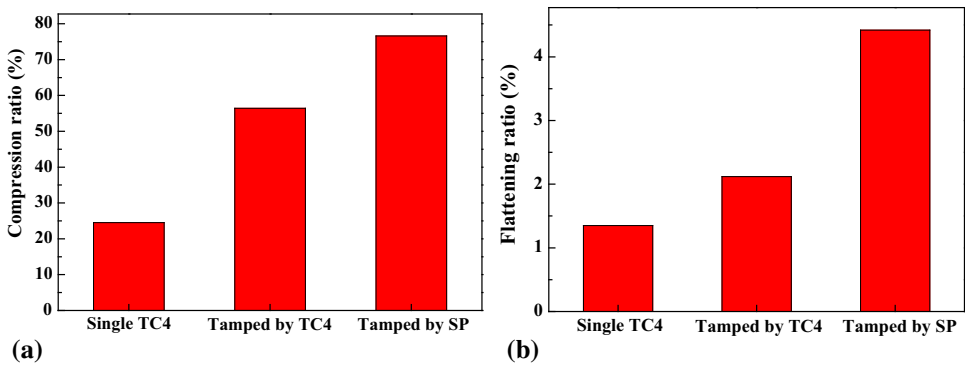

Fig. 4 Compression ratio (a) and flattening ratio (b) of previously deposited TC4 particle under three cases

height of the particle to the original diameter, and the calculation of flattening ratio used the equivalent diameter method (Ref 33). As can be seen in Fig. 4, after the subsequent impact of TC4 particle and large peening particle, the compression ratio was increased by 133 and 216%, respectively. The flattening ratio of the previously deposited TC4 particle was increased by 57 and 227%, respectively. Therefore, the tamping effect of the subsequent impacts, particularly with the large shot particle, played a significant role in increasing the deformation of the originally deposited particle due, with the shot particle's effect being largest due to its increased kinetic energy.

Interface Temperature

Figure 5 plots the temperature distribution on the particle interface in the three cases. It can be seen that the highest temperature when a single TC4 particle impacted the substrate was 1452 K, and the area with the highest temperature was mainly distributed around the edge of the particle with relatively large deformation. After impact by a following TC4 particle, the maximum temperature reached 1553 K, distributed in the area of the interface between particle and substrate. After being tamped by the shot particle, the maximum temperature of the deposited particle reached 2090 K, with the high temperature mainly distributed in two regions: the bottom area where the particle deformed the most and the top area impacted by the shot particle. The increase in interface temperature stems from the heat of the plastic deformation caused by the increased deformation from shot peening.

Figure 6 displays the temperature distribution diagram of the bottom and top surfaces of the particle in the three cases. It can be seen in the figure that when a single TC4 particle impacted the substrate, the high-temperature region was mainly distributed on the bottom edge of the particle and the highest temperature was 1452 K. The width of the highest-temperature region was approximately 1.48 μm, the sub-high temperature was 1356 K, and the width was approximately 1.21 μm. In the case of secondary impact of TC4 particle, the maximum temperature of the interface reached 1553 K with the high-temperature region similarly located on the bottom edge, and the width of the highest-temperature and sub-high-temperature regions was approximately 0.72 and 0.8 μm, respectively. The width of the high-temperature zone on the bottom of the particle was not significantly different in these two cases. However,

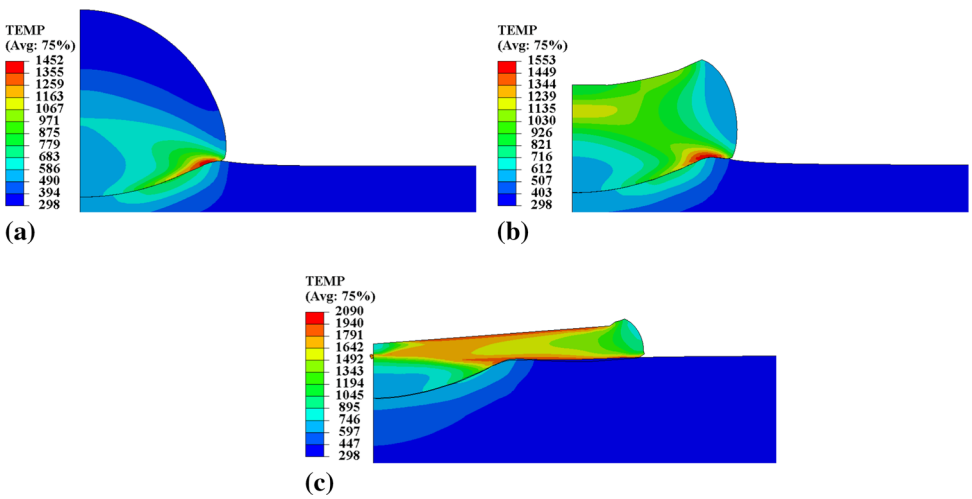

Fig. 5 The temperature contour under different conditions. (a) TC4 particle/TC4 substrate. (b) Impacted by subsequent TC4 particle. (c) Impacted by subsequent shot particle

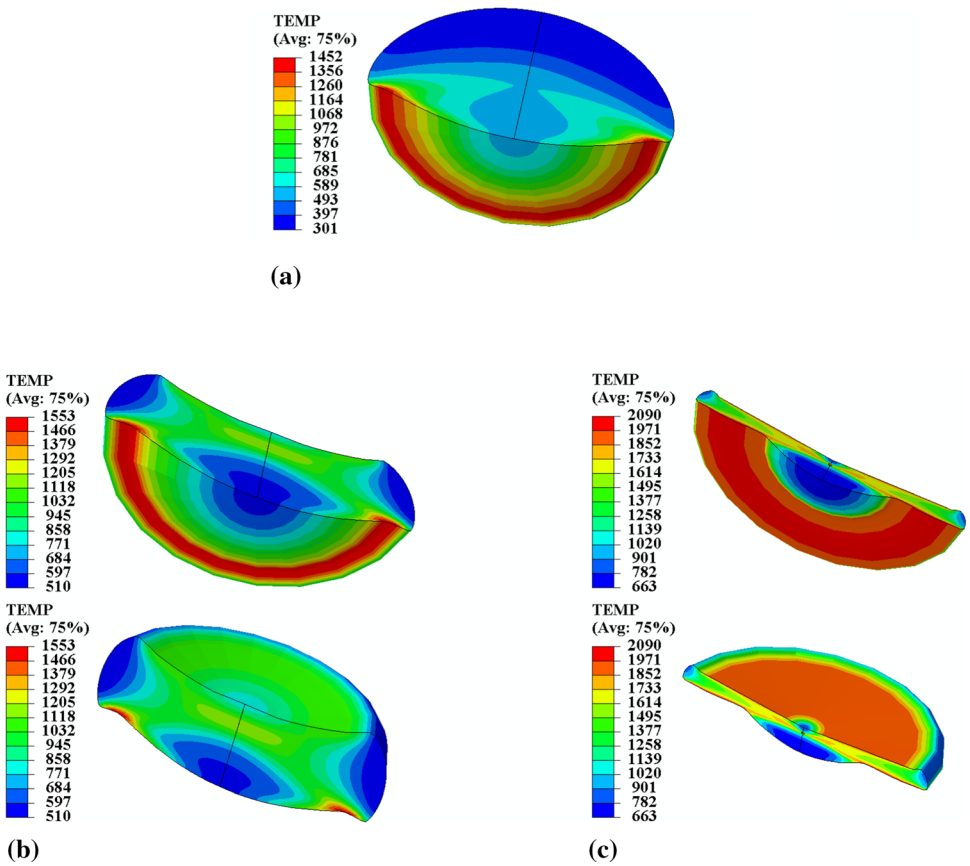

Fig. 6 The temperature contour on the bottom and top of the previously deposited TC4 particle. (a) TC4 particle/TC4 substrate. (b) Impacted by subsequent TC4 particle. (c) Impacted by subsequent shot particle

after being impacted by a large shot particle, the high-temperature zone expanded outward due to the severe deformation of the deposited particle. At the bottom of the particle, the highest and sub-high temperature reached 2090 and 1971 K, respectively. The width of the highest-temperature and sub-high-temperature zone was increased to approximately 2.56 and 8.42 μm, respectively. Moreover, on the surface of the particle, in the range of approximately 15.34 μm, the temperature reached 1971 K, which matched the sub-high temperature on its bottom edge. Compared with the single particle impact case, the highest observed temperature increased by approximately 638 K, and the sub-high temperature increased by approximately 519 K, while the width of the sub-high-temperature zone expanded by nearly six times. Importantly, the temperature in both the highest-temperature and the sub-high-temperature regions in the case of shot peening exceeded the melting point of 1878 K. The total width of the area above the melting point on the bottom of the particle reached approximately 11 μm, which implies that a wide area of the particle melted after shot impact. Effective bonding is likely to happen here, which can improve the bonding strength (Ref 34). In addition, the particle surface melted in a large range which was not seen in the case of an impact by a subsequent TC4 particle. The large melting area on the particle surface will make it easier to deform when impacted by subsequent particles.

Figure 7 shows temperature distribution contours in the substrate surface in the three model cases. From the substrate side, the highest-temperature zone mainly appeared in the area contacted by the particle. In the case of a single particle, the highest temperature was 805 K and the width of the highest-temperature zone was approximately 3.72 μm; the sub-high temperature toward the center was 785 K and the width of this zone was approximately 1.67 μm. After impact by the subsequent TC4 particle and the shot particle, the highest temperature reached 785 and 777 K, respectively, which is not very different from the first case; therefore, it can be concluded that the impact of subsequent TC4 particle and shot particle had almost no influence on the substrate temperature.

Figure 8 shows the change of temperature and strain over time at the selected node under the three conditions. As can be seen in Fig. 8, in the case of a single TC4 particle impact, the equivalent stress of the particle increased rapidly within a very short time (less than 10 ns) due to the strain hardening caused by instantaneous deformation. At the same time, the interface temperature soared rapidly, from 298 K to more than 1200 K in approximately 10 ns, and up to a maximum of 1384 K. Correspondingly, with

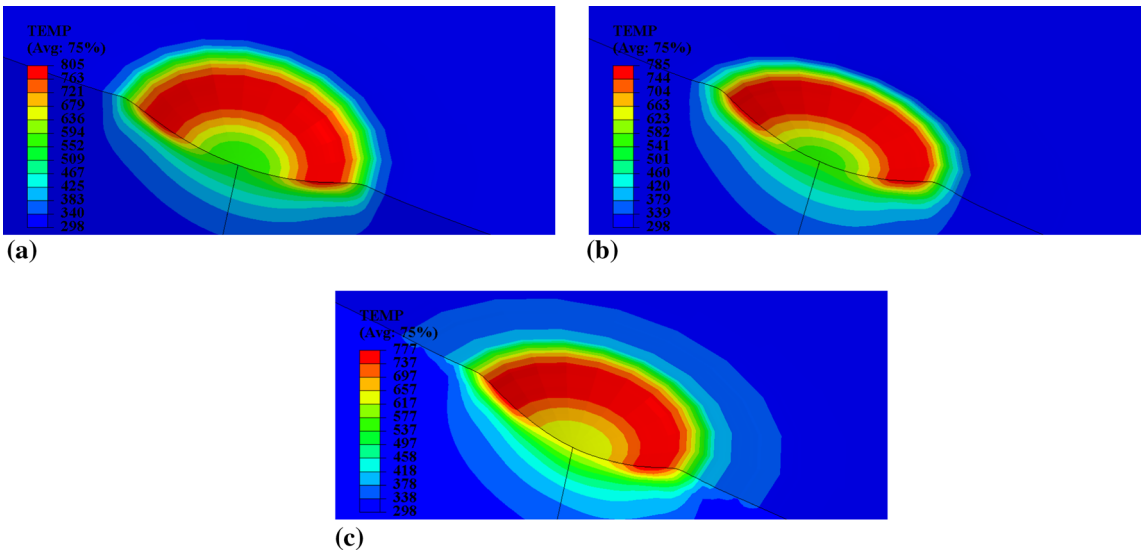

Fig. 7 The temperature contour on the surface of the substrate. (a) TC4 particle/TC4 substrate. (b) Impacted by subsequent TC4 particle. (c) Impacted by subsequent shot particle

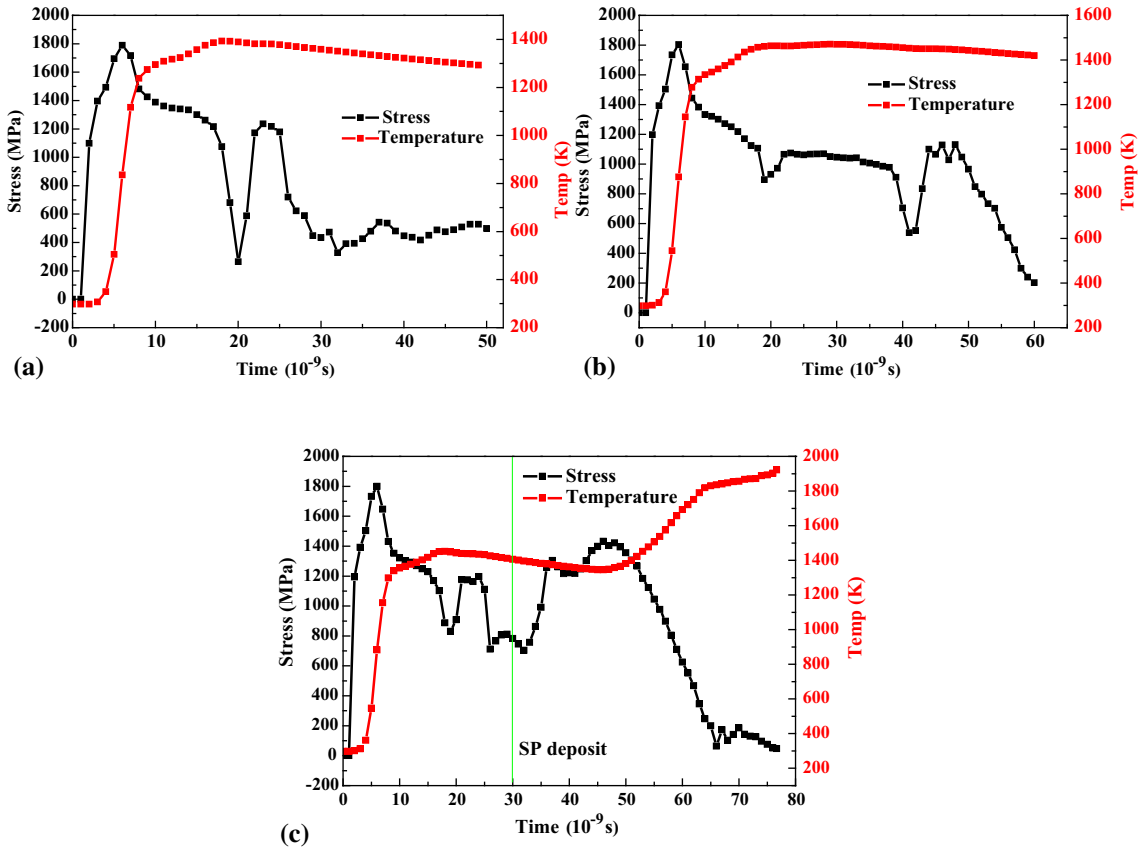

Fig. 8 The temperature and strain over time at selected node. (a) TC4 particle/TC4 substrate. (b) Impacted by subsequent TC4 particle. (c) Impacted by subsequent shot particle

increasing temperature, thermal softening occurred, and the stress dropped from a maximum of 1789 MPa to a minimum of 327 MPa. However, this temperature is still far away from the melting point of the TC4, which is approximately 1878 K. Therefore, particle melting does not occur under this condition. In cold spraying, due to the high particle velocity, the particle undergoes high-strain viscoplastic deformation within a short time (Ref 12). The

high temperature at the interface will cause local thermal softening, resulting in a rapid decrease in equivalent stress (Ref 10, 11). Although the thermal softening of the particle provides favorable conditions for further deformation after subsequent impact of the following particles, the residual stress is still very high, and there was a fluctuation of stress of approximately 30 ns, which indicates that the possibility of rebound is still very high and the bonding state between the particle and substrate is not stable (Ref 7, 35).

Meanwhile, when a subsequent TC4 particle impacted on the deposited TC4 particle, the interface temperature at the selected node increased to 1470 K. Correspondingly, the stress dropped from the maximum of 1803-538 MPa, followed by a degree of recovery that may be caused by the strain hardening resulting from the subsequent impact. Then, the stress continued to decrease before stabilizing at approximately 202 MPa. In the case of secondary tamping by a peening particle, the stress and temperature of the deposited TC4 particle underwent secondary change after a short, relatively stable period. It can be seen in Fig. 8(c) that due to the velocity difference between TC4 and peening particle, after the previously TC4 particle completed the first deformation, the peening particle then came into contact with it at approximately 30 ns. The peening particle continued to move downward, thereby compelling the TC4 particle to be compressed again. Since the selected node was located at the bottom of the particle, and the deformation of the particle transmitted gradually from top to bottom, an "incubation period" existed that lasted for approximately 20 ns. During this period of time, the temperature at this node remained at a relatively stable level, whereas the stress fluctuated slightly. Before that, the equivalent stress decreased rapidly after the first deformation, followed by a certain degree of rebound that may have occurred due to the high temperature after the impact and the subsequent cooling, resulting in temporarily restoring the strength of the particle. However, after a short "incubation period," the temperature of deposited TC4 particle increased rapidly, exceeding the melting point within approximately 10 ns, reaching the maximum of 1922 K during the simulation period. Correspondingly, as the temperature increased, the equivalent stress decreased rapidly until it eventually became zero after the stress underwent a short period of recovery and stabilization. Therefore, the in situ tamping effect not only enhanced the deformation of the particle but also promoted the local melting of the previously deposited TC4 particle.

Marginal Plastic Strain

Figure 9 shows the strain on the specified path (from A to C in Fig. 1a) of the previously deposited TC4 particle over time in three cases. From Fig. 9(a), when single particle impacted the substrate, the particle began to undergo plastic deformation within 5 ns. With time, the particle deformation gradually increased, and there was a large up–down fluctuation in strain, which may be due to the extremely unstable deformation at this time. In addition, the location of the point, where the maximum plastic strain occurred, was constantly expanding from A to B; therefore, it can be indirectly inferred that the contact area between the particle and substrate was continuously increasing. After approximately 30 ns, the particle deformation tended to be stable. At this time, the length of the area where the particle was in contact with the substrate (shown by the arrow in the figure) was roughly equivalent to the particle radius, which is consistent with the results shown in Fig. 3(a).

When the subsequent TC4 particle impacted the deposited TC4 particle, the particle strain experienced a secondary increase along the peripheral semicircular path, and this increment in strain stabilized after approximately 50 ns, as shown in Fig. 9(b). This was mainly due to the secondary tamping effect of subsequent particle, which further increased the deformation of the particle and the contact area between the particle and substrate. However, such tamping effect caused by the following large shot particle was more obvious. In the in situ peening state, the shot particle took approximately 30 ns to reach the top of the deposited TC4 particle, and then, the particle underwent a "secondary deformation" after the first plastic deformation, as shown in Fig. 9(c). There was a short interval between these two deformations due to the velocity difference between TC4 and shot particle. After the interval period, the deformation in the upper half of the particle, near point C, soared rapidly due to the tamping effect of the large shot particle, causing the deposited particle to squeeze out to the edge, reaching the maximum value at 70 ns. The abovementioned temperature analysis suggests that the thermal softening caused by the local melting of the area, wherein the particle was in contact with the substrate, made the secondary deformation of the particle easier. As the particle deformation increased, the contact area between the particle and substrate also increased rapidly, as shown by the straight line with arrows. Compared with the non-shot peening state, the contact area between the particle and substrate increased significantly. In addition, by comparing the abscissas of these three figures, we can see that the length of the contact area between the particle and substrate did not exceed the half-circumference of the TC4

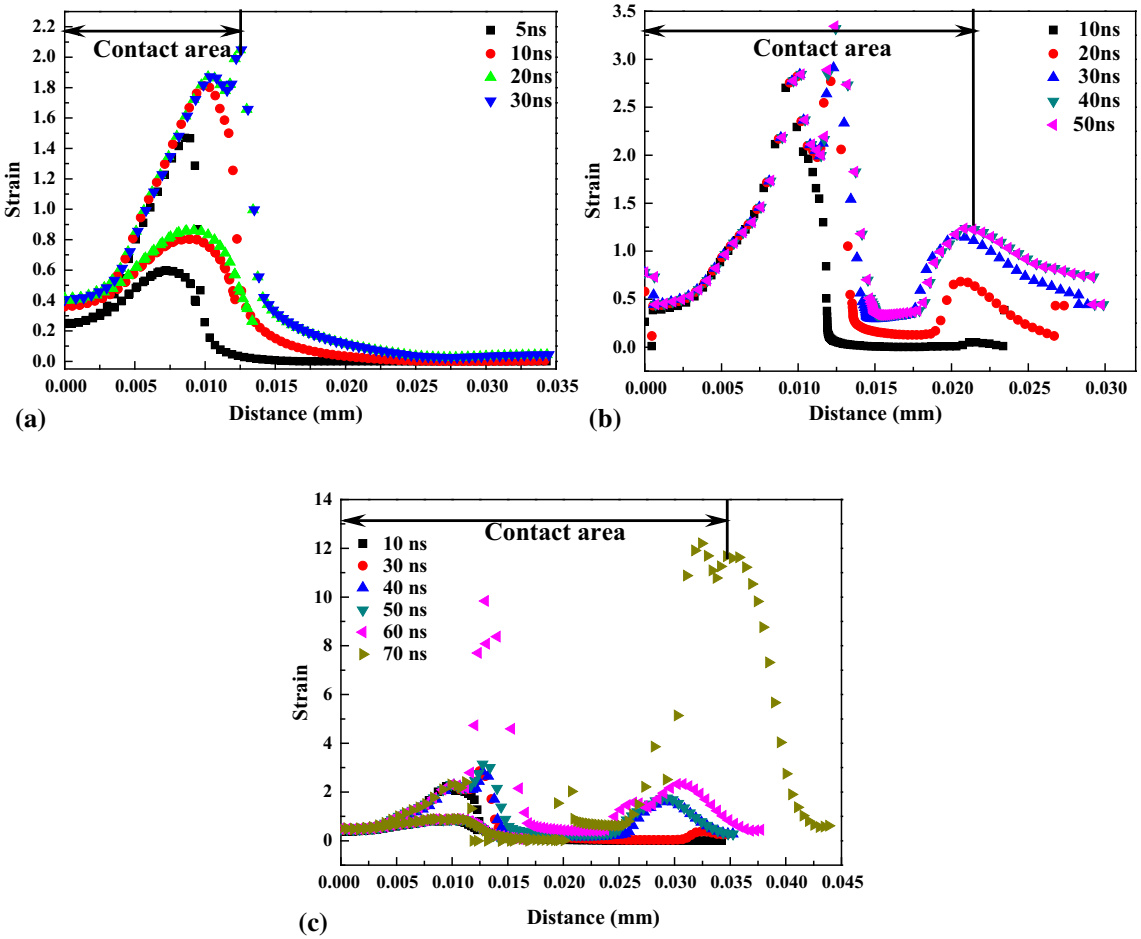

Fig. 9 The strain on the specified path over the time. (a) TC4 particle/TC4 substrate. (b) Impacted by subsequent TC4 particle. (c) Impacted by subsequent shot particle (two sets of points in a and b results from data fluctuation)

particle (approximately 0.035 μm) under the first two conditions. However, in the in situ peening state, the plastic deformation area extended beyond half of the circumference from 40 ns. Combined with the results of interface temperature, it was likely that the localized melting produced a viscous flow, which plays an important role in generating edge sputtering and improving bonding state (Ref 7).

Energy Analysis

During the cold-spraying process, the particle and substrate can be considered as a system. The initial kinetic energy of the in-fight particle is mainly converted into plastic deformation of particle and substrate (E_P), viscous effect (E_V), frictional heat (E_F), and recoverable elastic strain energy (E_R) in the contacting bodies. The conversion of energy during impact can be described as follows:

$$E = E_P + E_V + E_F + E_R \quad \text{(Eq 2)}$$

Among these four types of energies, plastic deformation energy accounts for the largest proportion, and only a few percent of the initial kinetic energy is normally dissipated as viscous effects and frictional heat; therefore, they can be ignored (Ref 6). In this way, by analyzing the change in the initial kinetic energy, plastic deformation energy, and recoverable elastic strain energy over the impact time, the bonding state of the particle and the substrate can be explained.

Figure 10 shows the initial kinetic energy, plastic deformation energy, and elastic recovery energy of previously deposited TC4 particle and substrate as a function of impact time. In the single particle impact state, the kinetic energy of the particle decreased quickly when it came into contact with the substrate. In contrast, the plastic deformation energy of the particle increased rapidly, almost at the same time, when the kinetic energy dropped to the bottom of the valley, plastic deformation energy reached the maximum, and recoverable elastic strain energy increased slightly with an increase in the plastic

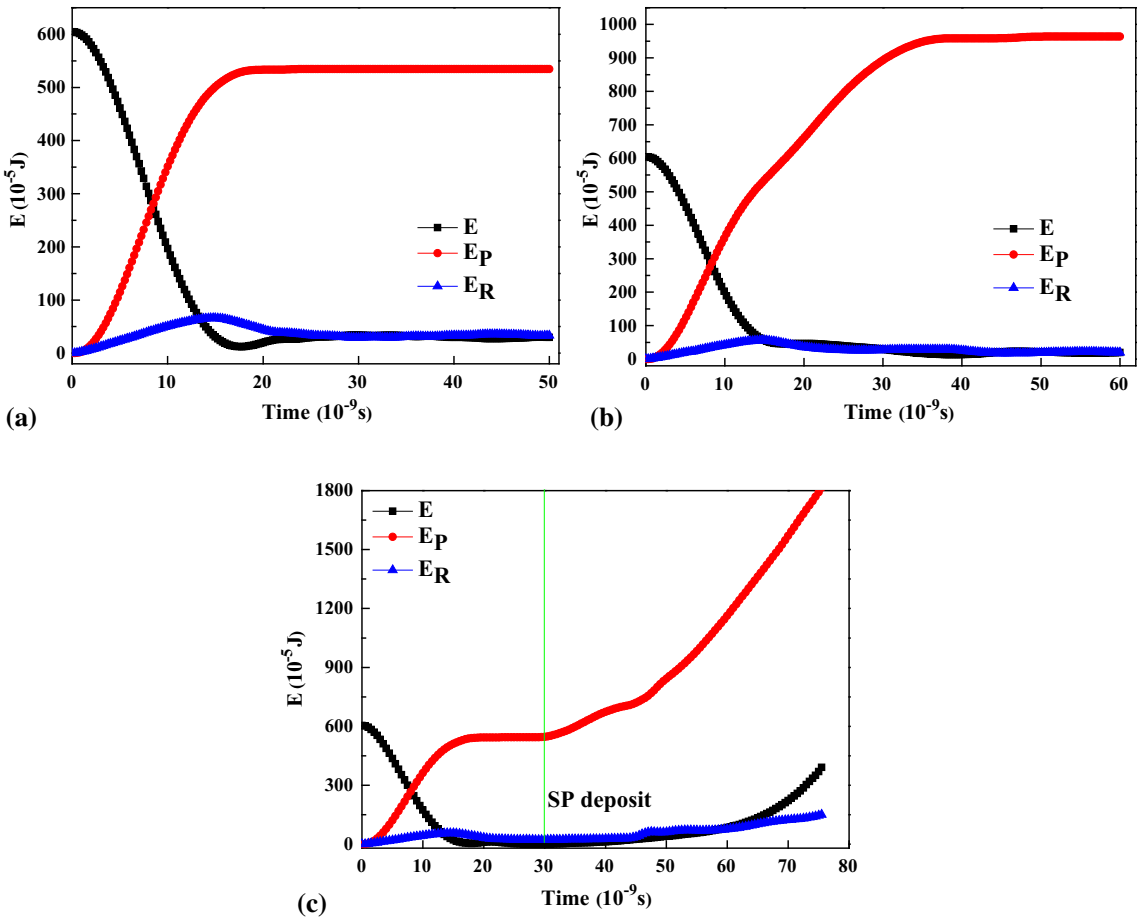

Fig. 10 The change of the energy in three cases. (a) TC4 particle/TC4 substrate. (b) Impacted by subsequent TC4 particle. (c) Impacted by subsequent shot particle

deformation energy. Then, it began to decrease after the plastic deformation energy stabilized and eventually remained at a level close to zero. Since the recoverable elastic strain is the energy source for the particle rebound, the lower the elastic recovery energy, the smaller the possibility of the particle rebound, thereby suggesting that the particle and substrate effectively bond with each other.

In the subsequent TC4 particle secondary impact state, the plastic deformation of particle continued to increase, i.e., approximately 1.7 times the maximum value than that of the single particle impact state. Furthermore, the influence of subsequent particle impact on the plastic deformation of deposited particle is significant. Moreover, in the case of in situ shot peening, the plastic deformation energy of the deposited TC4 particle experienced a secondary rise when the shot particle reached it, the plastic deformation energy continued to increase almost in a straight line. Obviously, it was the secondary tamping effect of the large shot particle that promoted further deformation of previously deposited particle. Simultaneously, the kinetic energy and elastic recovery energy of the particle experienced a plateau of approximately 20 ns after falling to the bottom of the valley, followed by a slow recovery. This may have resulted from the horizontal recovery to the particle center because of the large plastic deformation under external force of large shot particle.

Discussion

In cold spraying, the impact of subsequent particles has an in situ compaction effect on the plastic deformation of the deposited particles (Ref 13, 36). However, this self-compaction effect also has an impact on the bonding of the deposited particles. G. Bae et al. (Ref 37) have studied the effect of strain accumulation and thermal conduction during cold-sprayed CP-Ti coating. They found that the particle strain and temperature continued to increase during the coating formation. Similarly, in this study, we also found that the interface temperature exceeded melting temperature point after the subsequent shot peening particle impact. Therefore, the abovementioned results are

sufficient to confirm that the impact of subsequent particles on the interface parameters cannot be ignored during the particle deposition in cold spraying. Since the bonding state of the deposited particle cannot be identified easily in simulation, we can indirectly judge the particle bonding by the recoverable elastic strain energy. In this study, after the TC4 particle underwent subsequent collision, the change in recoverable elastic strain energy of earlier deposited TC4 particle can be shown in Fig. 11. Obviously, the recoverable elastic strain energy of the deposited TC4 particle after subsequent collision was lower than that of single particle state, indicating that the strain accumulation and thermal conduction resulting from subsequent particle collision during cold spraying is beneficial for bonding.

During cold spraying, the flying particle impacts substrate at a very high velocity, followed by deforming in nanoseconds. The substantial deformation area always focuses on the particle's periphery (in the jetting region), while almost no deformation occurred in the center of the particle (Ref 32). Therefore, the temperature at the rim area is significantly higher than that at the center of the particle, and edge instability is much easier to occur. In many cases, this instability was associated with a thin interface layer with temperature approaching or exceeding the melting point of the material. Several previously conducted studies (Ref 6, 38, 39) have noted the correlation between the morphologies and the rapid temperature increase (adiabatic heating) exhibited by a deforming particle in cold spraying. In contrast, interface melting is relatively easy to occur in material with low melting point as Sn and Zn, even in metallic glass coatings (Ref 40, 41). In the research of cold-sprayed Zn coating (Ref 40), some small spherical particles were formed that resulted from particle melting during high velocity impact followed by rapid cooling.

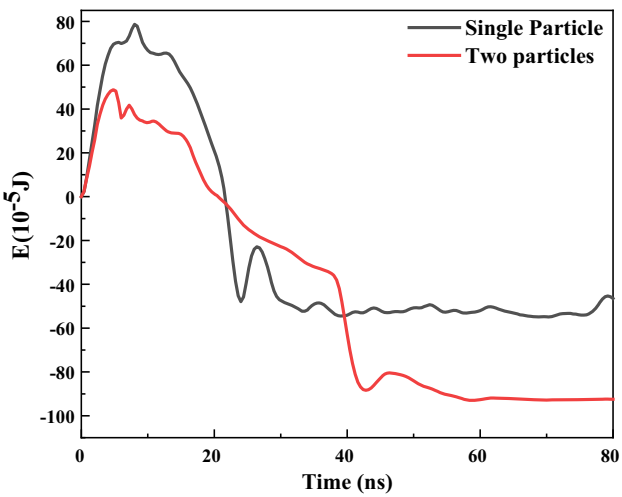

Fig. 11 Recoverable elastic strain energy over the impact time under cases of single and two TC4 particles

In cold spraying, most of the plastic deformation energy of the particle is converted into plastic heat. Therefore, the interface temperature increases rapidly within a few nanoseconds. For soft materials such as Cu and Al, due to severe jetting and high thermal conductivity, the plastic heat is relatively easy to dissipate. However, for Ti and Ti alloys, because of high strength and low thermal conductivity, there is no serious edge jetting and heat transformation. Bae et al. (Ref 7) proposed for the first time that there may be an interface melting phenomenon during the cold spray deposition of Ti and Ti alloys. Fig. 12 shows the viscous flow phenomenon observed at the interface of Ti coating, presumably due to the local melting of the interface. It was speculated that this interfacial melting caused by an increase in the local temperature will improve the particle–substrate and particle–particle metallurgical bonds.

Recently, some research have reported interface melting for Ti and Ti alloys (Ref 42-44). In our previous research (Ref 14), we prepared the TC4 coating by in situ shot peening-assisted cold spraying. The results showed that the bonding strength of the coating was higher than that prepared under the traditional cold spraying with similar spraying parameters, and it has even exceeded the highest bonding strength value of Ti alloy coating reported so far. By analyzing the fractural morphology, a "shear lip" was found at the particle-to-particle interface, as shown in Fig. 13. Based on the above simulation results, we speculated that this "shear lip" most likely resulted from the local interface melting and molten particle flowing out to the periphery under the shearing effect of the impact. As mentioned above, the stress in this region was significantly decreased, whereas the temperature increased rapidly. Therefore, the thermal softening reduced the flow stress of the material in the periphery zone and overcame the strain and strain-rate hardening, further resulting in viscous flow to extrude (Ref 10, 12). The generation of this viscous flow is beneficial for the removal of oxide film on the particle surface, as well as the diffusion of atoms and chemical reactions between the viscous fluid and solid surface (Ref 45, 46). Therefore, it will be helpful for the bonding the particles. Because the interfacial melting phenomenon is difficult to observe in experiments, the current research in this field needs to be further deepened.

Conclusion

In this study, the impact behavior of a single TC4 particle, as well as the subsequent impact of another TC4 particle and shot particle, was analyzed via numerical simulation. The conclusions are as follows:

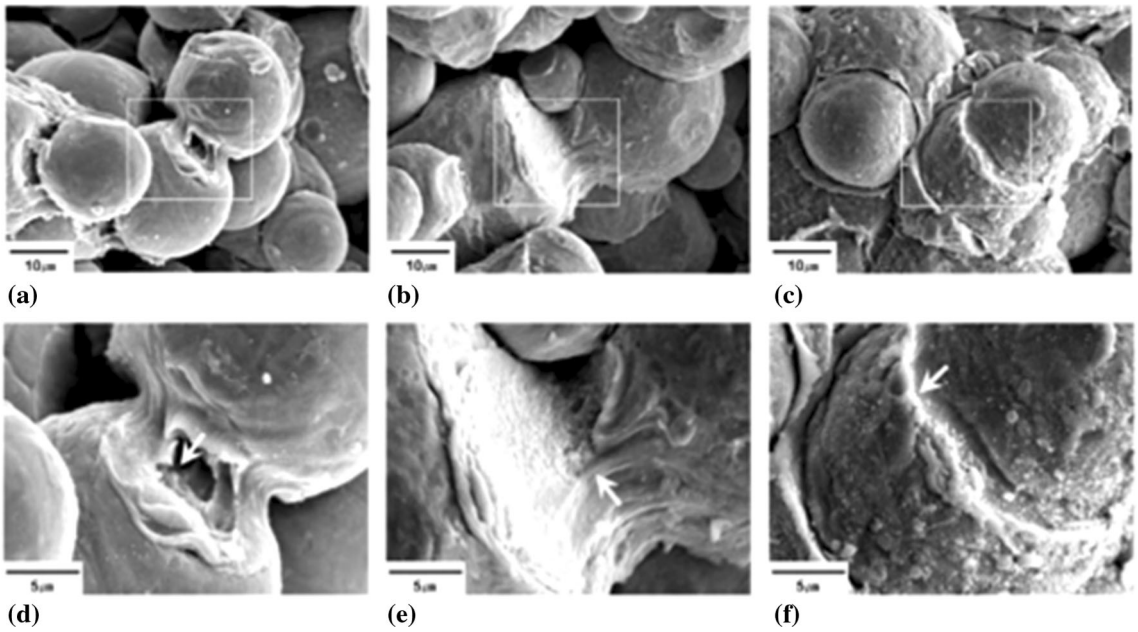

Fig. 12 Interface melting in cold-sprayed Ti coating (Ref 7). (a) Nitrogen, 600 °C, 2.5MPa. (b) Nitrogen, 600 °C, 2.5MPa, powder feeder gas preheating temperature at 600 °C. (c) Helium, 600 °C, 1.5MPa. (d-f) Higher magnifications of the boxed areas in (a-c)

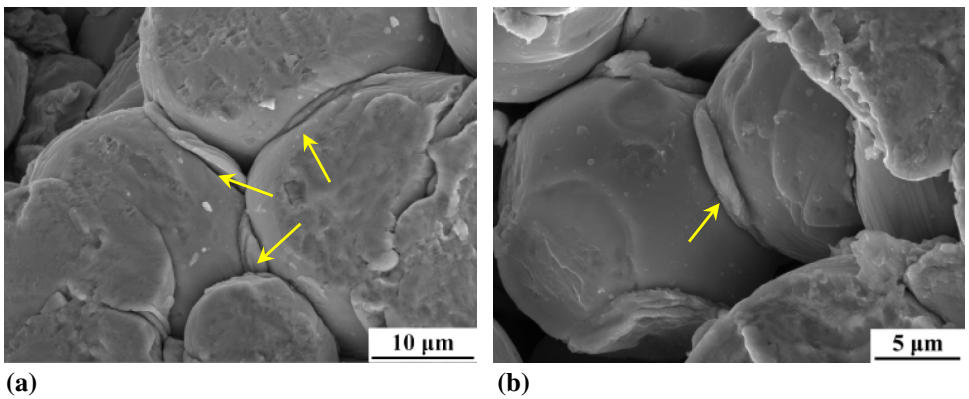

Fig. 13 Fracture morphologies of TC4 coatings: (a) N_2, 700 °C, 3 MPa; and (b) N_2, 750 °C, 3 MPa (Ref 14)

1. In the case of a single TC4 particle, when the particle impacted the substrate at a velocity of 700 m/s, only limited deformation occurred in the lower half of the particle. After the subsequent TC4 particle impact, the previously deposited particle underwent further deformation and the contact area with substrate expanded. Meanwhile, significant secondary deformation occurred when a large shot particle impacted the particle, and the compression ratio and flattening ratio were increased by 2-3 times than that in the single particle case.
2. The change in interface temperature over impact time under three cases showed that the highest temperature under single particle state was 1452 K, and the highest-temperature zone was mainly distributed in the limited area near the particle edge. In the case of subsequent TC4 particle impact, the temperature increased slightly. However, after the impact by the shot particle, the maximum interface temperature exceeded the melting point of Ti material, molten area was predicted, and the contact area between particle and substrate further increased.
3. In the three cases, the strain of selected node on the edge of the particle increased with an increase in the impact and then showed a tendency to fluctuate. Simultaneously, the node temperature increased rapidly, thereby confirming that the thermal softening reduced the strain hardening of the particle and improved the plastic deformability.

Acknowledgments The authors would like to thank the financial support by the National Science Fund of China (No. 51761145108) and Youth Foundation of National Natural Science Fund of China

(No. 52001180). Support for ABAQUS software was provided through University of Nottingham.

References

1. H. Assadi, H. Kreye, F. Gärtner and T. Klassen, Cold Spraying—A Materials Perspective, *Acta Mater.*, 2016, **116**, p 382–407.
2. D. Goldbaum, J. Michael Shockley, R.R. Chromik et al., The Effect of Deposition Conditions on Adhesion Strength of Ti and Ti6Al4V Cold Spray Splats, *J. Thermal Spray Technol.*, 2012, **21**(2), p 288–303.
3. R. Dykhuizen, M. Smith, D. Gilmore, R. Neiser, X. Jiang and S. Sampath, Impact of High Velocity Cold Spray Particles, *J. Therm. Spray Technol.*, 1999, **8**(4), p 559–564.
4. M. Grujicic, J.R. Saylor, D.E. Beasley, W.S. Derosset and D. Helfritch, Computational Analysis of the Interfacial Bonding Between Feed-Powder Particles and the Substrate in the Cold-Gas Dynamic-Spray Process, *Appl. Surf. Sci.*, 2003, **219**(3–4), p 211–227.
5. S. Barradas, R. Molins, M. Jeandin, M. Arrigoni, M. Boustie, C. Bolis, L. Berthe and M. Ducos, Application of Laser Shock Adhesion Testing to the Study of the Interlamellar Strength and Coating-Substrate Adhesion in Cold-Sprayed Copper Coating of Aluminum, *Surf. Coat. Technol.*, 2005, **197**(1), p 18–27.
6. G. Bae, Y. Xiong, S. Kumar, K. Kang and C. Lee, General Aspects of Interface Bonding in Kinetic Sprayed Coatings, *Acta Mater.*, 2008, **56**(17), p 4858–4868.
7. G. Bae, S. Kumar, S. Yoon, K. Kang, H. Na, H.J. Kim and C. Lee, Bonding Features and Associated Mechanisms in Kinetic Sprayed Titanium Coatings, *Acta Mater.*, 2009, **57**(19), p 5654–5666.
8. Y. Xie, S. Yin, C. Chen, M.P. Planche, H. Liao and R. Lupoi, New Insights into the Coating/Substrate Interfacial Bonding Mechanism in Cold Spray, *Scr. Mater.*, 2016, **125**, p 1–4.
9. Y. Xiong, K. Kang, G. Bae, S. Yoon and C. Lee, Dynamic amorphization and recrystallization of metals in kinetic spray process, *Appl. Phys. Lett.*, 2008, **92**(19), p 194101.
10. M. Grujicic, C.L. Zhao, W.S. Derosset and D. Helfritch, Adiabatic Shear Instability Based Mechanism for Particles/Substrate Bonding in the Cold-Gas Dynamic-Spray Process, *Mater. Des.*, 2004, **25**(8), p 681–688.
11. T. Schmidt, F. Gärtner, H. Assadi and H. Kreye, Development of a Generalized Parameter Window for Cold Spray Deposition, *Acta Mater.*, 2006, **54**(3), p 729–742.
12. H. Assadi, F. Gartner, T. Stoltenhoff and H. Kreye, Bonding Mechanism in Cold Gas Spraying, *Acta Mater.*, 2003, **51**(15), p 4379–4394.
13. X.-T. Luo, Y.-K. Wei, Y. Wang and C.-J. Li, Microstructure and Mechanical Property of Ti and Ti6Al4V Prepared by an In-Situ Shot Peening Assisted Cold Spraying, *Mater. Des.*, 2015, **85**, p 527–533.
14. H. Zhou, C. Li, G. Ji, S. Fu, H. Yang, X. Luo, G. Yang and C. Li, Local Microstructure Inhomogeneity and Gas Temperature Effect in In-Situ Shot-Peening Assisted Cold-Sprayed Ti-6Al-4V Coating, *J. Alloys Compd.*, 2018, **766**, p 694–704.
15. Oyinbo S.T., Jen T.C., Investigation of the process parameters and restitution coefficient of ductile materials during cold gas dynamic spray (CGDS) using finite element analysis. Add. Manuf. 31
16. Oviedo, F., Valarezo, A. Residual Stress in High-Velocity Impact Coatings: Parametric Finite Element Analysis Approach. J. Thermal Spray Technol. 1–21 (2020)
17. S. Yin, P. He, H. Liao and X. Wang, Deposition Features of Ti Coating Using Irregular Powders in Cold Spray, *J. Therm. Spray Technol.*, 2014, **23**(6), p 984–990.
18. S. Yin, X.-F. Wang, W.-Y. Li and B.-P. Xu, Numerical Investigation on Effects of Interactions Between Particles on Coating Formation in Cold Spraying, *J. Therm. Spray Technol.*, 2009, **18**(4), p 686–693.
19. D. Goldbaum, R.R. Chromik, N. Brodusch and R. Gauvin, Microstructure and Mechanical Properties of Ti Cold-Spray Splats Determined by Electron Channeling Contrast Imaging and Nanoindentation Mapping, *Microsc. Microanal.*, 2015, **21**(3), p 570–581.
20. M. Grujicic, C.L. Zhao, W.S. Derosset and D. Helfritch, Adiabatic Shear Instability Based Mechanism for Particles/Substrate Bonding in the Cold Gas Dynamic Spray Process, *Mater. Des.*, 2004, **25**(8), p 681–688.
21. P.C. King, G. Bae, S.H. Zahiri, M. Jahedi and C. Lee, An Experimental and Finite Element Study of Cold Spray Copper Impact onto Two Aluminum Substrates, *J. Thermal Spray Technol.*, 2009, **19**(3), p 620–634.
22. K.H. Kim, M. Watanabe and S. Kuroda, Bonding Mechanisms of Thermally Softened Metallic Powder Particles and Substrates Impacted at High Velocity, *Surf. Coat. Technol.*, 2010, **204**(14), p 2175–2180.
23. S. Yin, X.F. Wang, B.P. Xu and W.Y. Li, Examination on the Calculation Method for Modeling the Multi-Particle Impact Process in Cold Spraying, *J. Therm. Spray Technol.*, 2010, **19**(5), p 1032–1041.
24. E.H. Kwon, S.H. Cho, J.W. Han, H.L. Chang and H.J. Kim, Particle Behavior in Supersonic Flow During the Cold Spray Process, *Met. Mater. Int.*, 2005, **11**(5), p 377–381.
25. G.R. Johnson and W.H. Cook, A Constitutive Model and Data for Metals Subjected to Large Strains, High Strain Rates and High Temperatures, *Eng. Fract. Mech.*, 1983, **21**, p 541–548.
26. S. Yin, X. Suo, Z. Guo, H. Liao and X. Wang, Deposition Features of Cold Sprayed Copper Particles on Preheated Substrate, *Surf. Coat. Technol.*, 2015, **268**, p 252–256.
27. Y.-F. Wang and Z.-G. Yang, Finite Element Model of Erosive Wear on Ductile and Brittle Materials, *Wear*, 2008, **265**(5–6), p 871–878.
28. Lesuer, D., Experimental investigation of material models for Ti-6Al-4V and 2024-T3. https://e-reports-ext.llnl.gov/pdf/236167.pdf. Accessed 29 Dec 2015 (2000)
29. Kay, G., *Failure modeling of titanium 6AI-4V and aluminum 2024-T3 with the Johnson-Cook material model*. 2003: Office of Aviation Research, Federal Aviation Administration.
30. X. Wang and J. Shi, Validation of Johnson-Cook Plasticity and Damage Model Using Impact Experiment, *Int. J. Impact Eng*, 2013, **60**, p 67–75.
31. R. Kapoor and S. Nemat-Nasser, Determination of Temperature Rise During High Strain Rate Deformation, *Mech. Mater.*, 1998, **27**(1), p 1–12.
32. M.V. Vidaller, A. List, F. Gaertner, T. Klassen, S. Dosta and J.M. Guilemany, Single Impact Bonding of Cold Sprayed Ti-6Al-4V Powders on Different Substrates, *J. Therm. Spray Technol.*, 2015, **24**(4), p 644–658.
33. G. Sundararajan, N.M. Chavan and S. Kumar, The Elastic Modulus of Cold Spray Coatings: Influence of Inter-Splat Boundary Cracking, *J. Therm. Spray Technol.*, 2013, **22**(8), p 1348–1357.
34. J. Pan, S. Hu, A. Niu, K. Ding and L. Yang, Numerical Analysis of Particle Impacting and Bonding Processes During High Velocity Oxygen Fuel Spraying Process, *Appl Surf Ence*, 2016, **366**, p 187–192.

35. J. Wu, H. Fang, S. Yoon, H. Kim and C. Lee, The Rebound Phenomenon in Kinetic Spraying Deposition, *Scr. Mater.*, 2006, **54**(4), p 665–669.
36. L.I. Chang-jiu and L.I. Wen-ya, Microstructure Evolution of Cold-Sprayed Coating During Deposition and Through Post-Spraying Heat Treatment, *Trans. Nonferrous Metals Soc. China*, 2004, **14**(2), p 49–54.
37. G. Bae, K. Kang, J.-J. Kim and C. Lee, Nanostructure Formation and Its Effects on the Mechanical Properties of Kinetic Sprayed Titanium Coating, *Mater. Sci. Eng. A*, 2010, **527**(23), p 6313–6319.
38. C. Borchers, T. Schmidt, F. Gärtner and H. Kreye, High Strain Rate Deformation Microstructures of Stainless Steel 316L by Cold Spraying and Explosive Powder Compaction, *Appl. Phys. A*, 2007, **90**(3), p 517–526.
39. Papyrin, A., *The Cold Spray Materials Deposition Process||The development of the cold spray process*. 2007.
40. C.-J. Li, W.-Y. Li and Y.-Y. Wang, Formation of Metastable Phases in Cold-Sprayed Soft Metallic Deposit, *Surf. Coat. Technol.*, 2005, **198**(1–3), p 469–473.
41. S. Yoon, G. Bae, Y. Xiong, S. Kumar, K. Kang, J.J. Kim and C. Lee, Strain-Enhanced Nanocrystallization of a CuNiTiZr Bulk Metallic Glass Coating by a Kinetic Spraying Process, *Acta Mater.*, 2009, **57**(20), p 6191–6199.
42. M. Saleh, V. Luzin and K. Spencer, Analysis of the Residual Stress and Bonding Mechanism in the Cold Spray Technique Using Experimental and Numerical Methods, *Surf. Coat. Technol.*, 2014, **252**, p 15–28.
43. P.C. King, C. Busch, T. Kittel-Sherri, M. Jahedi and S. Gulizia, Interface Melding in Cold Spray Titanium Particle Impact, *Surf. Coat. Technol.*, 2014, **239**, p 191–199.
44. W.-Y. Li, C. Zhang, X. Guo, C.-J. Li, H. Liao and C. Coddet, Study on Impact Fusion at Particle Interfaces and Its Effect on Coating Microstructure in Cold Spraying, *Appl. Surf. Sci.*, 2007, **254**(2), p 517–526.
45. T. Stoltenhoff, H. Kreye and H. Richter, An Analysis of the Cold Spray Process and Its Coatings, *J. Therm. Spray Technol.*, 2002, **11**(4), p 542–550.
46. H.J. Kim, C.H. Lee and S.Y. Hwang, Fabrication of WC–Co Coatings by Cold Spray Deposition, *Surf. Coat. Technol.*, 2005, **191**(2–3), p 335–340.